Analysis of a continuous-time adaptive voter model

Emmanuel Kravitzch[*] and Yezekael Hayel[†]
Laboratoire Informatique d'Avignon (LIA), Avignon Université, F-84000 Avignon, France

Vineeth S. Varma[‡]
Département Contrôle Identification Diagnostic (CID), Université de Lorraine, CNRS, CRAN, F-54000 Nancy, France

Antoine O. Berthet[§]
Laboratoire des Signaux et Systèmes (L2S), Université Paris-Saclay, CNRS, CentraleSupélec, F-91190 Gif-Sur-Yvette, France

(Received 14 December 2022; accepted 6 May 2023; published 25 May 2023)

In this paper, we study a variant of the voter model on adaptive networks in which nodes can flip their spin, create new connections, or break existing connections. We first perform an analysis based on the mean-field approximation to compute asymptotic values for macroscopic estimates of the system, namely, the total mass of present edges in the system and the average spin. However, numerical results show that this approximation is not very suitable for such a system, for which it does not capture key features such as the network breaking into two disjoint and opposing (in spin) communities. Therefore, we propose another approximation based on an alternate coordinate system to improve accuracy and validate this model through simulations. Finally, we state a conjecture dealing with the qualitative properties of the system, corroborated by numerous numerical simulations.

DOI: 10.1103/PhysRevE.107.054307

I. INTRODUCTION

A. Research context and literature review

In the last decades, models of statistical mechanics have been extensively studied to describe a wide spectrum of complex phenomena, ranging from ferromagnetism to biochemical interactions. Social systems and collective phenomena are also under the scope of the aforementioned framework. In this case, the particles are agents that influence each other according to simple rules. One of the main models is a spin system called the voter model (VM) introduced by Liggett [1] and defined as follows. Consider a population of agents of size K and index by an integer k each agent, $k \in [\![1, K]\!]$. At all times $t \geqslant 0$, each agent k is endowed with a binary value $X_k(t) \in \{+1, -1\}$. These two values represent two opposite orientations that may be opinions, consumer preferences, behaviors, etc. Across time, the agents may change their spin under the influence of others, leading to a *stochastic process*. Since Liggett's seminal work, the VM has attracted a lot of attention and numerous refinements have been explored, e.g., nonlinear VMs [2], with stubborn agents [3] or contrarian [4], including noise [5]. A comprehensive survey can be found in Ref. [6].

By the way, the word *voter* should be taken in a very abstract sense: It may actually model any situation where some agents have to make a repeated choice between several possibilities, here two for sake of simplicity. Specifically, in the context of social networks, the main mechanisms shaping the social dynamics are *social mimetism*, *homophily,* and *selective exposure*. Social mimetism is the behaving trend involving synchronization of one's own opinions with those of the imitated person. Homophily is the trend one has to connect with alike people—alike simply means having the same spin in the VM formalism. Analogously, selective exposure is the trend one has to dismiss dissonant neighbors, that is, agents having an opposite spin. These notions have been thoroughly described by psychosocial studies [7,8] and then taken for granted in this paper. While VMs over *static* graphs encompass social mimetism, they fail to encompass selective exposure and homophily. To keep track of these last two key characteristics, we have to consider a model where the graph is *adaptive*, evolving according to the spin profile $(X_k)_{k\in[\![1,K]\!]}$. Models of this kind are said to be *coevolutionary* [9] or *adaptive* and are the focus of this paper. Though more recent and less studied than systems over static graphs, adaptive voter models (AVMs) are the subject of growing interest, e.g., in the context of epidemics [10]. By allowing the edges to evolve, a wide choice of network dynamics is worth considering. Some authors define a local linkage mechanism [11,12], called *triadic closure* or *transitivity reinforcement*, where agents only seek new friends among their two-hop neighbors. Nevertheless, the main model is the one proposed in Ref. [13], with two possible opinions. It is an AVM with a simple linking rule: When agent l breaks his tie with agent m,

[*]emmanuel.kravitzch@alumni.univ-avignon.fr
[†]yezekael.hayel@univ-avignon.fr; https://sites.google.com/site/yezekaelhayelsite/
[‡]vineeth.satheeskumar-varma@univ-lorraine.fr; https://sites.google.com/site/vineethshome/
[§]antoine.berthet@centralesupelec.fr

he immediately reconnects to another agent p, the latter being uniformly chosen over the whole population (*rewire to random)*. See, for instance, Refs. [14,15] and references therein. Sometimes, rewiring is done only among like-minded people, that is, people of the same spin (*rewire to same*). Finally, some authors recently integrated AVMs as building blocks into an evolutionary game-theoretic framework [16,17]. In the context of cooperation and defection, it is indeed appealing to generalize game models to dynamical networks and this modification may display different behaviors compared to games over static networks. Here again, the authors choose rewiring to random with global linkage, namely, the basic and most popular model in the literature. Hence, making the link between game theory and adaptive networks is an additional motivation to investigate several instances of AVMs. The main difference in the model studied here is that breaking and linking are done simultaneously, hence the total mass of edges is conserved. The refinement we propose is to allow edge breaks and edge creations separately. In this model, the degree distribution is then dynamic, increasing the range of possible configurations. In particular, the degree distribution can evolve.

B. Motivation and main contributions

Among the traditional questions raised by such statistical mechanics models, the most classical one is that of the *phase transition*. It is well-known that in VMs, several radically different regimes can be observed, depending on the model's parameters: In the case of static graphs, the two types of spins can survive—this case is mentioned as *coexistence* in Ref. [1], also called the *metastable* regime; or, on the contrary, one spin can rapidly conquer all the agents: In this case, we talk about *consensus*. After reaching consensus, the dynamics stops; consensus is said to be an *absorbing* configuration. When defining the model's parameters, there are a range of values dedicated to each of the phases and there exists (surface of) values at the boundary, hence the term *phase transition*. In the case of adaptive networks, the situation is a bit different. One may have clustering according to the spins. Thus, both spins are preserved but the two clusters are completely separated. On the contrary, a third possibility is the coexistence of disagreeing agents among the same connected components. In this case, some links between the two communities of spins, named *discordant* links and properly defined in the sequel, maintains. Hence, global consensus is simply a very particular case of the first scenario.

In this paper, instead of tracking threshold values for phase transitions, as done in Ref. [18], we rather strive to give qualitative results about the macroscopic behavior of the coupled dynamics. The main contributions are the following:

(1) In the dense graph regime, we highlight the homogeneous behavior and the existence of a continuous trajectory which might be the limiting system as $K \to +\infty$. It is notable that this phenomenon is independent of the model's parameters. Further investigations may uncover the very nature of this object.

(2) We also provide quantitative results: By a change of coordinates, we identify the surface of equilibria, and estimate the limiting discordance (namely the mass of discordant edges) for the metastable regime. This estimation shows very good results compared to the standard mean-field approximation applied to the natural edges-spins coordinates.

(3) Finally, a linearization based analysis of the reduced-order system around the points corresponding to absorbing states, provides a reasonable approximation of the phase transition that occurs in the initial stochastic system.

In the remainder of the paper, Sec. II presents the model. Section III analyzes the model using the standard mean-field approximation. Section IV refines the analysis by introducing a change of coordinates partitioning the edges into blocks. Section V formulates a conjecture and supports it with numerous numerical simulations. Section VI concludes the paper and indicates avenues for future research. The table below summarizes some notations.

Object definition	Formula	Symbol
Population index	$\{1, ..., K\}$	$[K]$
Unweighted digraph	$a_{lm} = 0$ or 1	A
Complete graph	$\mathbb{K}_{lm} = 1 \forall l, m \in [K]$	$\mathbb{K}$
Hadamard product	$(A \odot B)_{ij} = a_{ij} b_{ij}$	$\odot$
ith unitary vector of $\mathbb{R}^K$		e_i
0 matrix with 1 at only lm	$e_l e_m^T$	e_{lm}
All-1 vector	$\sum_j e_j$	$\mathbb{1}$
Indicator U	1 if U occurs, 0 else	$\mathbb{1}_U$

II. MODEL

Let us define a population of agents of size $K \geqslant 1$ evolving and interacting over time. At all times $t \geqslant 0$, each agent $k \in \{1, ..., K\}$ (denoted by $[K]$ for short) is endowed with a binary value $X_k(t) = \pm 1$ called a *spin*. The spin can represent an orientation, a preference, or any other individual state. The term "spin" comes from the analogy with magnetization models and is already used in early works on VMs over lattices. We then keep it throughout the text by commodity. The vector $X(t) := (X_k(t))_{k \in [K]} \in \{+1, -1\}^K$ is the *spin profile* at time t. The agents interact through a dynamic graph $\mathcal{G}_t$, the latter *coevolving* with the spin profile. Throughout this paper, graph $\mathcal{G}_t$, supposed to be unweighted and directed, is represented by its adjacency matrix $A(t) \in \{0, 1\}^{K^2}$. We have that $a_{lm}(t) = 1$ if and only if there is a link from agent l to agent m at time t. We will also use the generalized notation: For two subsets $U, V \subset [K]$ we denote by $a_{UV} := \sum_{l \in U, m \in V} a_{lm}$.

The overall process (X^K, A^K) (the dependence in K will be omitted when it is clear from the context) then evolves in the finite state space: $\mathcal{S}_K := \{+1, -1\}^K \times \{0, 1\}^{K^2}$. The rates associated to the coevolution dynamics, namely, the nodes' dynamics and the edges are now introduced. The dynamics of the agents' spins correspond to the standard linear VM, already abundantly analyzed over regular lattices (Chap. V of [1] and part II of Ref. [19]) and more recently over heterogeneous and random graphs [20,21]. It models the mimetic behavior of individuals. Typically, an agent with positive spin (value $+1$) surrounded by agents displaying negative spin (value -1) is very likely to flip because of the influence of

the neighbors. The flip rate of agent $k \in [K]$ is given by

$$\text{flip: } (X, A) \longrightarrow (X - 2X_k e_k, A) \text{ at rate}$$
$$\Phi(k; X, A) = \phi \sum_{j \in [K]} A_{kj} \mathbb{1}_{(X_k \neq X_j)}, \tag{1}$$

where e_k is the kth unit vector of $\mathbb{R}^K$. The voter step is said to be linear because the rate to flip is linear with respect to the number of disagreeing neighbors. In this regard, the parameter $\phi > 0$ can be interpreted as the persuadability coefficient, equal for all agents.

On top of this linear flip dynamics, we consider the following edge dynamics. It takes into account two important properties that are characteristic of social interactions, namely, *homophily* and *selective exposure*. As mentioned in the Introduction, they, respectively, correspond to the trend one has to create links with alike people on one hand and to dismiss disagreeing neighbors on the other hand. These two features have been copiously described by psychosocial studies [7,22] and are nowadays well recognized to play a structural role in social dynamics. Then, for any individuals $l, m \in [K]$, the rate for link creation and link deletion (when it exists) are respectively defined as follows:

$$\text{link creation: } (X, A) \longrightarrow (X, A + e_{lm}) \text{ at rate}$$
$$\Gamma(lm; x, A) = \gamma(1 - A_{lm}) \underbrace{\mathbb{1}_{(X_l = X_m)}}_{\text{homophily}}, \tag{2}$$

where one shall remember that we are dealing with a *directed* graph and $e_{lm} = e_l e_m^T$ is the unitary matrix with a 1 at entry (l, m) and only 0's everywhere else, and

$$\text{link deletion: } (X, A) \longrightarrow (X, A - e_{lm}) \text{ at rate}$$
$$B(lm; x, A) = \beta A_{lm} \underbrace{\mathbb{1}_{(X_l \neq X_m)}}_{\text{selec. exposure}}, \tag{3}$$

where γ (respectively, β) is the propensity of one agent l to get connected (respectively, disconnected) to another agent m endowed with the same spin (respectively, with opposite spin).

For any $f : \mathcal{S}_K \mapsto \mathbb{R}$, the associated generator $Q : \mathbb{R}^{\mathcal{S}_K} \mapsto \mathbb{R}^{\mathcal{S}_K}$ allows us to characterize the Markov process by a single formula. Then,

$$\begin{aligned}(Qf)(x, a) = &\sum_k \Phi(k; x, a)[f(x - 2e_k x_k, a) - f(x, a)] \\ &+ \sum_{lm} \Gamma(lm; x, a)[f(x, A + e_{lm}) - f(x, a)] \\ &+ \sum lmB(lm, x, A)[f(x, a - e_{lm}), f(x, a)].\end{aligned} \tag{4}$$

Note that if the rate parameters ϕ, γ, and β are in the same range, the agents' spin dynamics (1) is, therefore, K times faster compared to the edge stones given by (2) and (3). Since we are interested in the coevolution of the two dynamics (spin and graph) at the *same timescale*, from now on we consider that the flip rate is in the same range as the others and thus $\phi = O(\gamma/K)$. The Markov process (X^K, A^K) can equivalently be described by a set of *stochastic differential equations* driven by $3K^2$ independent Poisson point processes $\mathcal{N}_{kj}^{\alpha}$ of intensity α with $(k, j) \in [K]^2$ and $\alpha \in \{\frac{\phi}{K}, \beta, \gamma\}$:

$$\begin{cases} dX_k(t) = -2X_k(t^-) \sum_j A_{kj}(t^-) \mathbb{1}_{(X_k(t^-) \neq X_j(t^-))} \mathcal{N}_{kj}^{\phi/K}(dt) \\ dA_{lm}(t) = (1 - A_{lm}(t^-)) \mathbb{1}_{(X_l(t^-) = X_m(t^-))} \mathcal{N}_{lm}^{\gamma}(dt) \\ \qquad\qquad - A_{lm}(t^-) \mathbb{1}_{(X_l(t^-) \neq X_m(t^-))} \mathcal{N}_{lm}^{\beta}(dt). \end{cases} \tag{5}$$

A. Absorbing configurations

When K is finite, it is clear that the VM over static (and adaptive) graphs possesses absorbing configurations (sometimes called *frozen states*), which can be identifiable. In our setting, the Markov process (X^K, A^K) indeed admits the following absorbing states:

$$\mathcal{A} = \{(x, a) \in \mathcal{S}_K : \forall (l, m), (x_l = x_m \text{ and } a_{lm} = 1) \tag{6}$$
$$\text{or } (x_l \neq x_m \text{ and } a_{lm} = 0)\}. \tag{7}$$

In other words, an absorbing state is then a configuration where the population of individuals is clustered in two separated complete subgraphs denoted by C^+ and C^- with $C^+ \bigcup C^- = [K], C^+ \bigcap C^- = \emptyset$, with $x_l = +1 \ \forall l \in C^+$ and $x_k = -1 \ \forall k \in C^-$, and with no links between the two blocks: $a_{ij} = a_{ji} = 0 \ \forall i \in C^+, \ \forall j \in C^-$.

Furthermore, the absorbing configurations are strongly attractive: With probability one, the process gets trapped into one of them after a (random) finite time T_{abs} defined as

$$T_{abs} := \inf\{t : (X(t), A(t)) \in \mathcal{A}\} < \infty. \tag{8}$$

B. Filter bubbles and discordance

When the stochastic process (X, A) has reached an absorbing state, then it stops: Each agent X_k has ultimately chosen his spin and has broken all of his links with the opposite individuals. This configuration represents the emergence of so-called *filter bubbles*: Each one confines himself to a group of people sharing the same opinion, and then has no access to other viewpoints, hence the term *filter bubble*. This phenomenon is suspected to increase radicalization and fake news propagation [23–25]. Detecting and forecasting the emergence of these bubbles is a major issue in social network analysis. A simple estimator to quantify the filter bubble effect is the *discordance* (sometimes called interface density [5]). This value measures how strongly two opposite communities influence one other. An edge lm is said to be *discordant* if $a_{lm} \mathbb{1}_{(x_l \neq x_m)} = 1$, meaning that a link between individuals l and m exists and the two individuals have opposite spin.

Definition 1 (total discordance). The total discordance $\mathcal{D}(x, a)$ of any configuration $(x, a) \in \mathcal{S}_K$ is defined as

$$\mathcal{D}(x, a) := \frac{1}{K^2} \sum_{lm} a_{lm} \mathbb{1}_{(x_l \neq x_m)}. \tag{9}$$

If $\mathcal{D}(x, a) = 0$, then it means that (x, a) is close to an absorbing configuration: The node dynamics has stopped, and after the link creation between agreeing agents, the overall process (X, A) will get frozen. Let us define the associated hitting time $T_{abs} := \inf\{t > 0 : \mathcal{D}(X(t), A(t)) = 0\}$. The following property, called *slow extinction* [26], properly formalizes metastability.

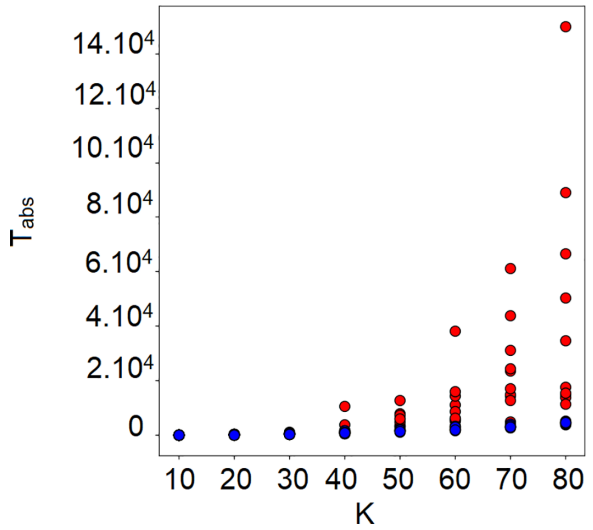

FIG. 1. Extinction time of the process for different number of agents $K = 10, 20, ..., 80$. In each case, ten simulations have been performed for each regime: In blue, the subcritical regime: $(\phi, \beta, \gamma) = (1, 1, 1)$; in red, the metastable one: $(\phi, \beta, \gamma) = (4, 1, 4)$. One can see that the absorbing time T_{abs} grows much faster in the metastable regime than in the subcritical regime.

Definition 2 (slow extinction). The total discordance *slowly becomes extinct* if

$$\exists c > 0, \quad \mathbb{P}(T_{abs} < e^{cK}) < e^{-cK}. \tag{10}$$

Figure 1 illustrates this phenomenon: We have plotted the extinction time evolution in terms of time to extinction for two different regimes: The subcritical regime ($\phi \approx \beta$, in blue), and the metastable regime ($\phi \gg \beta$, in red). It is clear that extinction time grows much faster for the metastable regime compared to the subcritical regime.

The next section is devoted to a first line of analysis, namely, one of the standard mean-field approximation.

C. Graph dynamics under a dense regime

Before turning our attention to the analysis, let us give a few words on the graph regime of the model defined so far. In network models, the density of links is indeed a structural attribute of the considered graph. For instance, many threshold results concerning Erdös-Renyi graphs deal with the *sparse regime* $\text{ER}(K, \frac{p}{K})$, $K \longrightarrow +\infty$ and $p > 0$ (see, for instance, part II of Ref. [27]). More recently, dense regimes have been intensively investigated and the field has then reached maturity [28]. It is the last frame that the current paper pertains to, where almost all nodes are connected to a significant proportion of all the other agents. This is due to the so-called edgecentric model design: Focus on agent $k \in [K]$, at time instant $t \in \mathbb{R}_+$, all concordant inactive links $\{kj : X_k(t) = X_j(t)$ and $a_{kj}(t) = 0\}$ activate at rate γ regardless of the other variables, without degree limitation. To this title, Fig. 2 illustrates the densification phenomenon: Fig. 2(a) plots several simulations where, initially, there is no concordant link: $a_{kj} = \mathbb{1}_{(X_k(0) \neq X_j(0))}$ and maximal discordance. Measuring

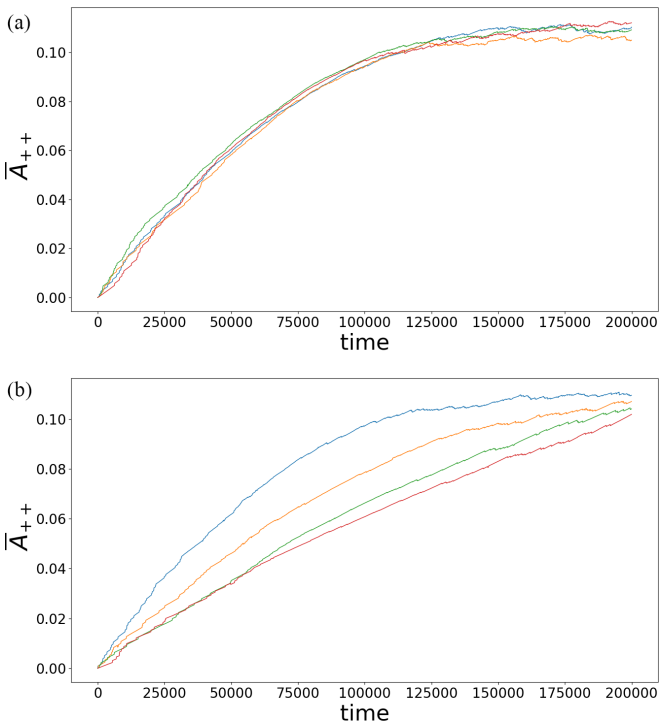

FIG. 2. (a) Evolution through time of the mass of concordant links between agents possessing positive spins normalized by the size of the block $\overline{A}_{++}$. We have made four simulations with $K = 500$ and $(\phi, \beta, \gamma) = (4, 1, 4)$ and with a concordant-free configuration at initial time. We observe that the four curves are very similar and they quickly grow to a stationary value $\sim$0.1. This confirms that the component of positive spin becomes dense very fast. (b) The same quantity $\overline{A}_{++}$ with all the same values, with the exception of β, the breaking rate parameter which varies as follows: In blue $\beta = 1$, in orange $\beta = 2.5$, in green $\beta = 4$, and in red $\beta = 5, 5$. Although the growth rate decays when β increases, one still observes that the community of positive spins gets dense fast for various values of β.

the ratio of positive concordant links $\overline{A}_{++} := \frac{\sum_{l,m} a_{lm} \mathbb{1}_{(X_l = X_m = 1)}}{(\sum_j \mathbb{1}_{(X_j = 1)})^2}$, we see that this quantity quickly grows from 0 to roughly 0.1, regardless of the model's parameters [Fig. 2(b)]. Thus, it is then clear that the block of agents with spin positive is dense. From this, one can also expect that, though dynamic, the entire graph displays a high degree of connectivity. This aspect is nonetheless outside the scope of the paper, and all the reader has to keep in mind is that dynamics evolve under a *dense regime*.

III. A FIRST APPROXIMATION: THE CLASSICAL NIMFA

The principle of the N-intertwined mean-field approximation (NIMFA) [29] is to consider that when the number of particles in the system is high, independence between particles state emerges, and then we have $\mathbb{E}X_kX_j = \mathbb{E}X_k\mathbb{E}X_j$. Thus applying this approximation by considering large number of agents, we can assume that $\mathbb{E}A_{lm}(t)X_k(t) = \mathbb{E}A_{lm}(t)\mathbb{E}X_k(t)$. Introducing the variables $x(t) := \mathbb{E}X(t) \in [-1, 1]^K$, $a(t) := \mathbb{E}A(t) \in [0, 1]^{K^2}$, taking both lines of (5) under expectation $\mathbb{E}[.]$, and assuming independence between particles yields the

associated NIMFA system for (x, a):

$$\dot{x}_k = \frac{\phi}{K}\sum_j a_{kj}(x_j - x_k)$$

$$\dot{a}_{lm} = \gamma(1-a_{lm})\underbrace{\frac{1+x_l x_m}{2}}_{\text{homophily}} - \beta a_{lm}\underbrace{\frac{1-x_l x_m}{2}}_{\text{sel.exp.}}. \tag{11}$$

In matrix form, it reads

$$\dot{x} = \frac{\phi}{K}(A - \text{diag}(A\mathbb{1}))x$$

$$\dot{a} = \gamma(\mathbb{K} - a)\odot\frac{\mathbb{K}+xx^T}{2} - \beta a \odot \frac{\mathbb{K}-xx^T}{2}, \tag{12}$$

where $\text{diag}(u)$ is the diagonal matrix $(\text{diag}(u))_{lm} := u_l \mathbb{1}_{(l=m)}$, $u \in \mathbb{R}^K$, and $\odot$ is the Hadamard (matrix) product. Here, we have used the fact that $\mathbb{1}_{(p\neq q)} = \frac{1-pq}{2}$ for $p, q \in \{+1, -1\}$, implying

$$-2X_k A_{kj}\mathbb{1}_{(X_k\neq X_j)} = A_{kj}[X_j - X_k], \tag{13}$$

hence recognizing a Laplacian term for the spin evolution in (11). By this computation, we can clearly identify the *homophily* term as well as the *selective exposure* term in (11).

A. Analysis of the NIMFA system

The deterministic system (11) is easier to analyze than the initial large-scale stochastic system: We are able to derive the entire set of equilibria and determine their stability.

Proposition 3. Let $g := \frac{\gamma}{\beta}$. The set of attractive equilibria of the above dynamical system (11) is

$$\mathcal{S} = \{(x, a) : x = c\mathbb{1}, c \in [-1, 1], a = v_*(c, g)\mathbb{K}\}, \tag{14}$$

where $\mathbb{1}$ is the vector full of 1's: $\mathbb{1} = \sum_j e_j$ and

$$v_*(c, g) = \frac{1}{1 + \frac{1-c^2}{2g}}. \tag{15}$$

Furthermore, there exists a set of unstable equilibria:

$$\mathcal{U} = \{(x, a) : x_k = \pm 1 \forall k \text{ and } x_l = x_m \iff a_{lm} = 1 \text{ or } x_l \neq x_m \iff a_{lm} = 0\}. \tag{16}$$

Proof. First, suppose that the system has reached a consensus state: $x \in \{c\mathbb{1} : c \in [-1, 1]\}$. We automatically have $\dot{x} = 0$. At consensus, the graph evolution yields

$$0 = \gamma(\mathbb{K} - A) - \frac{\beta(1-c^2)}{2}A = v_*(c, g)\mathbb{K}, \tag{17}$$

with $v_*(c, g)$ given by (15). From this, we can conclude that there is only one graph at consensual equilibrium $x_k = c\forall k$.

Let us now take in the more general case $\dot{A} = 0_{K\times K}$ and $\dot{x} = 0_K$. Suppose first $a_{ij} > 0 \forall i, j$, and define the homophily matrix as

$$H(x) := \frac{\mathbb{K}+xx^T}{2}. \tag{18}$$

We then obtain

$$\begin{aligned} &\dot{a} = 0_{K\times K} \\ \iff\ & 0 = -a \odot \{\gamma H(x) + \beta(\mathbb{K} - H(x))\} + \gamma H(x) \\ \iff\ & a = f_\odot(H(x)), \end{aligned} \tag{19}$$

with

$$f(h) = \frac{\gamma h}{\gamma h + \beta(1-h)}, \tag{20}$$

and $f_\odot : [0, 1]^{K^2} \mapsto [0, 1]^{K^2}$ the associated entrywise map taking matrices as arguments. Note that f is monotonically strictly increasing, thus invertible. Therefore,

$$\begin{aligned} f_\odot^{-1}(a) = H(x) &\Rightarrow \mathcal{L}(a)\circ f_\odot^{-1}(a) = 0 \\ &\Rightarrow \sum_j a_{lj}[f^{-1}(a_{jm}) - f^{-1}(a_{lm})] = 0 \forall l, m. \end{aligned} \tag{21}$$

Now, *ad absurdum*, suppose it exists a column m and two lines $l, L \in [K]$ such that $a_{lm} < a_{Lm}$. Because f^{-1} is also strictly increasing, $a_{Lj}[f^{-1}(a_{jm}) - f^{-1}(a_{Lm})] \leqslant 0\ \forall j$, with at least one *strict* inequality for $j = l$. Thus, equality 21 cannot be verified for all l, m. This shows that $a_{lj} = c_j\ \forall l, j$, and then

$$\dot{x}_k = 0 \Rightarrow \sum_j c_j(x_j - x_k) = 0 \Rightarrow x = c\mathbb{1}, c \in [-1, 1]. \tag{22}$$

And by the analysis made in the consensus state, it implies that the only possibility for the graph is $A = v_*(c, g)\mathbb{K}$, $c \in [-1, 1]$.

Until now, we have supposed that $a_{lm} > 0\ \forall l, m$. Suppose now there exists at least one null coefficient: $a_{lm} = 0$. Then $\dot{a} = 0 \Rightarrow 1 + x_l x_m = 0 \iff x_l = x_m = \pm 1$. Without loss of generality, take $x_l = +1$ and $x_m = -1$. We have $a_{lj}(x_j - x_l) \leqslant 0$. This implies that either $x_j = x_l$ or $a_{lj} = 0$. Furthermore, in the case of $x_l = x_j = \pm 1$, we necessarily have $a_{lj} = 1$. The set $\mathcal{U}$ is thus well identified.

We now study the stability of all these equilibria. To show the attractiveness of $\mathcal{S}$, one can first notice that the phase space $[-1, 1]^K \times [0, 1]^{K^2}$ is compact. Then, every trajectory $\{(x(t), A(t)) : t \geqslant 0\}$ admits at least one accumulation point $(x^*, A^*) \in \mathcal{S}\bigcup\mathcal{U}$ for all initial datum $(x(0), A(0)) \in [-1, 1]^K \times [0, 1]^{K^2}$. Second, notice that there is a *diameter contraction*: $x_{\min}(t) := \min_k x_k(t)$ is increasing, while $x_{\max}(t) := \max_k x_k(t)$ is decreasing, provided it exists some $k \in [K]$ such that $\dot{x}(0) \neq 0$. Every accumulation is thus in $\mathcal{S}$: $\exists t_j \geqslant 0$, $||x(t_j) - c1_K|| < \epsilon$ and $||x(t) - c1_K|| < \epsilon$ for all $t \geqslant t_j$. This implies that for two distinct edges $e = lm$, $f = kj$,the edges dynamics are roughly the same. Indeed, rewrite (11) as

$$\begin{aligned} \partial_t a_{lm} &= -(\gamma h_{lm} + \beta(1 - h_{lm}))a_{lm} + \gamma h_{lm} \\ &= u_{lm}(t)a_{lm} + h_{lm}(t), \end{aligned} \tag{23}$$

where $u_{lm}(t) < 0\ \forall l, m, t$ and $h_{lm} = \frac{1+x_l x_m}{2}$. Each edge difference $(a_{lm} - a_{kj})$ evolves according to

$$\begin{aligned} \partial_t(a_{lm} - a_{kj}) &= u_{lm}(t)a_{lm} + h_{lm}(t) - (u_{kj}a_{kj} + h_{kj}) \\ &= u_{kj}(a_{lm} - a_{kj}) + \eta(t), \end{aligned} \tag{24}$$

where

$$\eta(t) = (v_{lm} - v_{kj}) + a_{lm}(u_{lm} - u_{kj}) \tag{25}$$

can be made arbitrarily small provided ϵ is chosen small enough. Recall $u_{lm} < -\min(\gamma, \beta)$. Hence,

$$\partial_t(a_{lm} - a_{kj}) \leqslant -\min(\gamma, \beta)(a_{lm} - a_{kj}) + \eta_0. \tag{26}$$

By comparison principle (see lemma 3.4 of chapter 3 of [30]), we have

$$(a_{lm} - a_{kj}) \leqslant \min(\gamma, \beta) \text{ for large enough } t. \quad (27)$$

This allows us to conclude that $A(t)$ converges to the set $\{vA : v \in [0, 1]\}$. The previous derivation provides a closed-form analytical expression of the value v_* as a function of the consensus value c reached by the spin profile. ■

Remark 4. The set of stable equilibria $\mathcal{S}$ is made up of a continuum of points independent of ϕ, while the unstable ones are just isolated points in the compact phase space $\Psi := [-1, +1]^K \times [0, 1]^{K^2}$. The points in set $\mathcal{U}$ correspond to the absorbing configurations of the initial stochastic system, where the system is maximally polarized and the discordance is zero.

The NIMFA method also gives as output a closed-form expression of the discordance. Let us first extend the definition of the discordance to continuous systems as

$$\mathcal{D}(x, a) := \frac{1}{K^2} \sum_{lm} a_{lm} \frac{1 - x_l x_m}{2}. \quad (28)$$

Corollary 5. Consider the system having reached the surface of equilibria computed in Proposition 3: $(x, a) \in \mathcal{S}$ which implies $x = c\mathbb{1}$ for some $c \in [-1, +1]$ and $a = v_*(c, g)\mathbb{K}$. Then discordance reads

$$\mathcal{D}(x, a) = v_*(c, g) \frac{1 - c^2}{2}, \quad (29)$$

where v_* is defined in Proposition 3.

Proof. Because by definition

$$\mathcal{D} = \frac{1}{K^2} \sum_{lm} a_{lm} \mathbb{1}_{(x_l \neq x_m)} = \frac{1}{2K^2} \sum_{lm} a_{lm}(1 - x_l x_m), \quad (30)$$

the result is straightforward in view of Proposition 3. ■

B. Numerical simulations

To represent visually the dynamics, the Markov process is reduced to three global estimators, namely,

$$\overline{X} := \frac{1}{K} \sum_j X_j,$$
$$\overline{A} := \frac{1}{K^2} \sum_{lm} A_{lm}, \text{ and} \quad (31)$$
$$D := \frac{1}{K^2} \sum_{lm} A_{lm} \mathbb{1}_{(X_l \neq X_m)}.$$

$\overline{X}$ is the mean spin profile, $\overline{A}$ is the global density of links, and D is the discordance. In Fig. 3, five trajectories are represented in the $\overline{X} - \overline{A}$ axis, with slightly different initial configurations. We can see that all the trajectories are quasiattracted by the consensual equilibria line analytically computed in Proposition 3, although a small but consistent gap subsists. In the second plot, three trajectories are represented in the $\overline{X} - D$ axis. Also, in that case, the theoretical NIMFA-based discordance seems similar yet quantitatively distinct.

Let us try to understand intuitively why this bias occurs. For this purpose, let us represent the asymptotic system

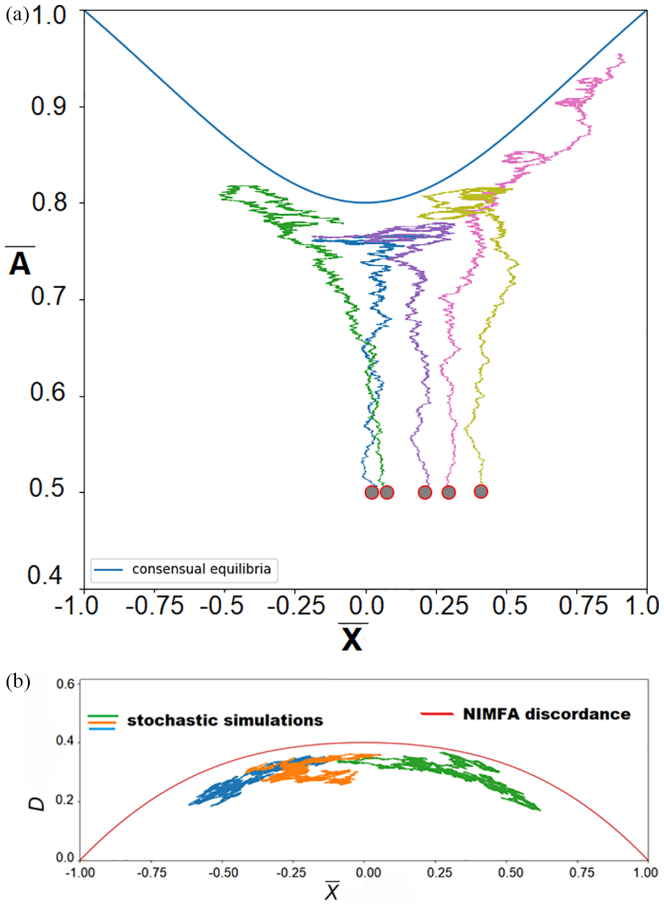

FIG. 3. Simulations have been performed in the metastable regime: $(\phi, \beta, \gamma) = (4, 1, 4)$ and $K = 800$. The grey points are the initial configurations. We see that the system is attracted by the blue curve analytically computed in Proposition 3, although there is still a small gap between the simulations and the theoretical result. A similar observation can be stated in part (b): we see that the three independent stochastic simulations have roughly the same shape as the theoretical NIMFA discordance line (in red), but here also a substantial gap persists.

$K \longrightarrow +\infty$ with a continuum of population $u \in [0, 1]$, and the associated spin profile and generalized matrix $\{X_u, A_{uv} : u, v \in [0, 1]\}$. This construction can be seen as the limiting system when $K \longrightarrow +\infty$. Informally, the NIMFA actually acts on it as follows: It makes a partition in an arbitrary fashion the population in K cells and applies a cellwise averaging:

$$x_j \sim \frac{1}{K} \int_{u \in I_j} X_u du, \quad a_{lm} \sim \frac{1}{K^2} \int_{(u,v) \in I_l \times I_m} A_{uv} du dv \quad (32)$$

for $j \in [K]$, with $I_j = [\frac{j}{K}, \frac{j+1}{K}[$. This is why we retrieve at the end a system of large though finite dimension. But this arbitrary averaging puts in the same category discordant links $\{(lm) : x_l \neq x_m\}$ and concordant links $\{(lm) : x_l = x_m\}$, leading to a dead-weight loss of information. To see this, let us take the following example: Suppose $x_l = x_m = 0$ and $a_{lm} = \frac{1}{2}$. This means that half the mass of cell l has a positive spin and the other half has a negative spin, and the same with cell m. Nonetheless, one cannot in any way determine whether the links from cell l to cell m are discordant or concordant, and

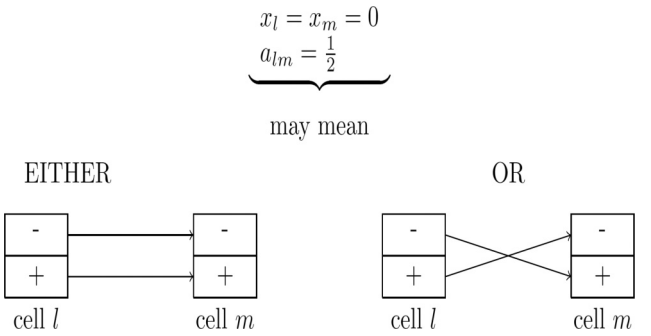

FIG. 4. In each cell l, m, a first half of the population is $+1$ and the other half is -1.

in which proportion. Thus, as depicted in Fig. 4, one of the drawbacks of the NIMFA is the ambiguity. It can correspond either to a case of discordance free: All agents of cell l are linked toward people in m of the same spin and *only* with them, or it can correspond to maximum discordance (and zero concordance) configuration. In the next section, an alternative system of coordinates is presented to make the distinction between concordant edges and discordant edges, and then assign distinct dynamics to these possible cases.

IV. NEW BLOCKWISE COORDINATE SYSTEM

Instead of considering the spin profile, let us just keep the graph structure. We separate the links in four categories $\mathcal{C}^1, \mathcal{D}^1, \mathcal{C}^0, \mathcal{D}^0 \in \{0,1\}^{K^2}$ according to two criteria: *concordant* ($\mathcal{C}$) or *discordant* ($\mathcal{D}$), and *present* (indexed with a one) or *absent* (indexed with a zero). This partition leads to the following equivalences:

$$\begin{aligned} a_{lm} = 1 \wedge x_l = x_m &\iff \mathcal{C}^1_{lm} = 1, \\ a_{lm} = 0 \wedge x_l = x_m &\iff \mathcal{C}^0_{lm} = 1, \\ a_{lm} = 1 \wedge x_l \neq x_m &\iff \mathcal{D}^1_{lm} = 1, \\ a_{lm} = 0 \wedge x_l \neq x_m &\iff \mathcal{D}^0_{lm} = 1. \end{aligned} \tag{33}$$

In this new coordinate system, the stochastic evolution equation is rewritten as

$$\begin{aligned} d\mathcal{C}^1 &= +\mathcal{C}^0 \odot \mathcal{N}^\gamma(dt) + (\mathcal{D}^1 - \mathcal{C}^1) \odot F(dt), \\ d\mathcal{C}^0 &= -\mathcal{C}^0 \odot \mathcal{N}^\gamma(dt) + (\mathcal{D}^0 - \mathcal{C}^0) \odot F(dt), \\ d\mathcal{D}^1 &= -\mathcal{D}^1 \odot \mathcal{N}^\beta(dt) + (\mathcal{C}^1 - \mathcal{D}^1) \odot F(dt), \\ d\mathcal{D}^0 &= +\mathcal{D}^1 \odot \mathcal{N}^\beta(dt) + (\mathcal{C}^0 - \mathcal{D}^0) \odot F(dt), \end{aligned} \tag{34}$$

where

$$F(dt) := (\mathcal{D}^1 \odot \mathcal{N}^{\frac{\phi}{K}}(dt)) \circ \mathbb{K} + \mathbb{K} \circ (\mathcal{D}^1 \odot \mathcal{N}^{\frac{\phi}{K}}(dt))^\top. \tag{35}$$

Here $\mathcal{N}^\alpha(t) = (\mathcal{N}^\alpha_{lm}(t))_{(l,m)\in[K]^2}$ is a square matrix of dimension K stacking all the independent Poisson processes of intensity $\alpha > 0$, $\alpha \in \{\frac{\phi}{K}, \beta, \gamma\}$. One can see that the first terms of the right-hand side correspond to the *network dynamics*, while the second terms correspond to the flip dynamics with the $\mathcal{N}^{\frac{\phi}{K}}$ as driving processes. Figure 5 provides a schematic

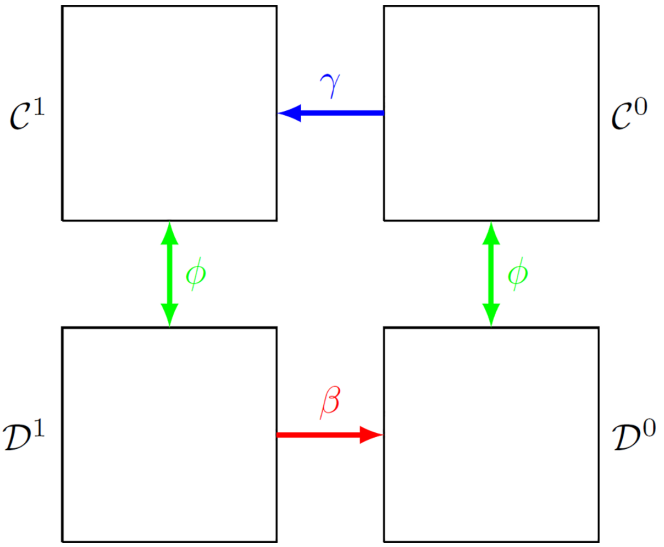

FIG. 5. A partition of the edges linked with flows.

picture of the different flows between the four compartments defined above.

A. Dimensionality reduction

System (34) describes the initial one (5) but from another viewpoint. Its main advantage is that it conveniently separates the discordant and concordant edges, and these two categories of edges display very different behaviors. It has to be noted that through these coordinates, one has no access to the mean spin profile $\overline{X}$ nor the proportion of agents with positive spin

$$m_+ := \frac{1}{K} \sum_j \mathbb{1}_{(X_j=1)}. \tag{36}$$

Because of its high dimensionality, actually $4K^2$, it seems intractable. Proposition 3 suggests to circumvent this difficulty by making the following *homogeneity hypothesis*:

$$\mathcal{C}^\sigma \approx c_\sigma \mathbb{K} \text{ and } \mathcal{D}^\sigma \approx d_\sigma \mathbb{K}, \tag{37}$$

for some $d_\sigma, c_\sigma \in [0,1], \sigma \in \{1,0\}$ with vanishing randomness when K gets large. Some details of this assumption will be given in the next section. The large-scale stochastic system (34) can then be described by a nonlinear four-dimensional deterministic ordinary differential equation (ODE):

$$\partial_t Y_t = \Psi(Y_t) = N_{\beta,\gamma} Y_t + 2\phi d_1 M Y_t, \tag{38}$$

where

$$Y = \begin{bmatrix} c_1 \\ c_0 \\ d_1 \\ d_0 \end{bmatrix}, N_{\beta,\gamma} := \begin{bmatrix} 0 & \gamma & 0 & 0 \\ 0 & -\gamma & 0 & 0 \\ 0 & 0 & -\beta & 0 \\ 0 & 0 & \beta & 0 \end{bmatrix} \tag{39}$$

and

$$M := \begin{bmatrix} -1 & 0 & +1 & 0 \\ 0 & -1 & 0 & +1 \\ +1 & 0 & -1 & 0 \\ 0 & +1 & 0 & -1 \end{bmatrix}. \tag{40}$$

Remark 6. Contrary to system (11) where the absorbing points are always unstable and repulsive regardless of the models' parameters, this system displays a stable discordance-free region for $\phi \ll \beta$:

Let us consider the discordance-free absorbing points that are easily identifiable:

$$\mathcal{A} = \left\{[u \quad 0 \quad 0 \quad 1-u]^T : u \in \left[\tfrac{1}{2}, 1\right]\right\}. \tag{41}$$

Setting $u = 1$ corresponds to a global consensus, while if $u = \frac{1}{2}$, then the two blocks are of the same size. By linearization of the vector field Ψ in (38), we get for $y \in \mathcal{A}$:

$$\partial\Psi_y = \begin{bmatrix} 0 & \gamma & -2\phi u & 0 \\ 0 & -\gamma & 2\phi(1-u) & 0 \\ 0 & 0 & -\beta + 2\phi u & 0 \\ 0 & 0 & \beta + 2\phi(u-1) & 0 \end{bmatrix}. \tag{42}$$

A simple examination of the eigenvalues leads to

$$\mathrm{Sp}\ \partial\Psi_y = \{0, 0, -\gamma, 2\phi u - \beta\}. \tag{43}$$

Furthermore, the null eigenvalue is semisimple. Then, by linearization method (Theorem 3.15 of Ref. [31]), for high enough β, that is, $\phi < \frac{\beta}{2u}$, the point y is stable.

Furthermore, system (38) being low dimensional, we can now give an explicit formula for the equilibria.

Proposition 7 (characterization of the equilibria). For any values ϕ, β, γ, in the coordinates (c_1, d_1, m), the surface of equilibria $\mathcal{S}_{eq}$ of the reduced system (38) is given by

$$\mathcal{S}_{eq} = \{(c_1, d_1, m_+) : d_1 = g(1 - c_1 - 2m_+(1-m_+))\}. \tag{44}$$

Proof. Recall $g := \frac{\gamma}{\beta}$. At equilibrium, $\partial_t Y = 0$, we have

$$d_1 = g c_0, \tag{45}$$

and by construction, $d_1 + c_1 + d_0 + c_0 = 1$ and $2m_+(1 - m_+) = d_0 + d_1$ at all times. Combining the last three identities yields the last proposition. ■

B. Computation of the discordance

We are now able to derive a formula for the global discordance d_1 at equilibrium: The third line of (38) yields

$$0 = -\beta d_1 + (c_1 - d_1)2\phi d_1. \tag{46}$$

Then, adding the first and second lines gives $0 = (d_1 - c_1 + d_0 - c_0)2\phi d_1$. Because $d_1 > 0$, we thus get

$$d_1 + d_0 = c_1 + c_0 = \tfrac{1}{2}. \tag{47}$$

Recall $d_1 = g c_0$, combining all the last identities allows us to state the following proposition.

Proposition 8. (Limit value for the discordance.) For high K, the discordance d_1 of system (X, A) converges toward the value $d^* = \frac{1}{2} \times \frac{1-\frac{\beta}{\phi}}{1+\frac{\beta}{\gamma}} \in [0, \frac{1}{2}]$.

Remark 9. This quantity does make sense only for $\phi > \beta$. More specifically, for $\phi \gg \beta$ and $\gamma \gg \beta$, d^* is almost maximal, namely, $d^* \approx \frac{1}{2}$. On the contrary, for $\beta < \phi$, the system is attracted toward the discordance-free region.

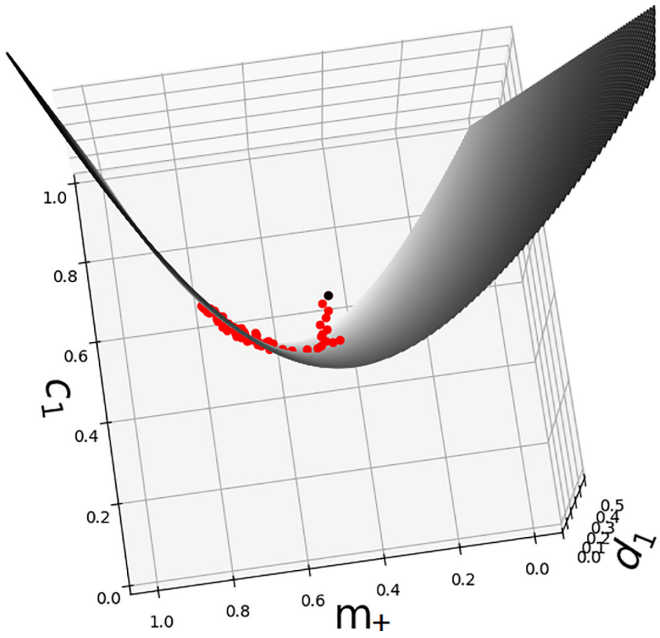

FIG. 6. $\mathcal{S}_{\mathrm{eq}}$ is represented by the grey surface. Red points are samples of the overall trajectory starting at the black point, under the metastable regime: $(\phi, \beta, \gamma) = (4, 1, 4)$ and $K = 800$. We see that there is no gap between the surface of theoretical surface and the stochastic simulation.

C. Numerical plots

Figure 6 shows how close the actual process is to the analytical surface $\mathcal{S}_{\mathrm{eq}}$ when projected to the phase space (c_1, m_+, d_1). Figure 7 displays four independent numerical simulations in the metastable regime with the same model's parameters. The horizontal line d^* corresponds to the value obtained in Proposition 8. When taking smaller ϕ, we observe that discordance is vanishing; see Fig. 8.

V. DISCUSSION

The results of the preceding section rely on the *homogeneity assumption* obtained by the standard NIMFA method (see Proposition 3). Because the spins and edges are binary

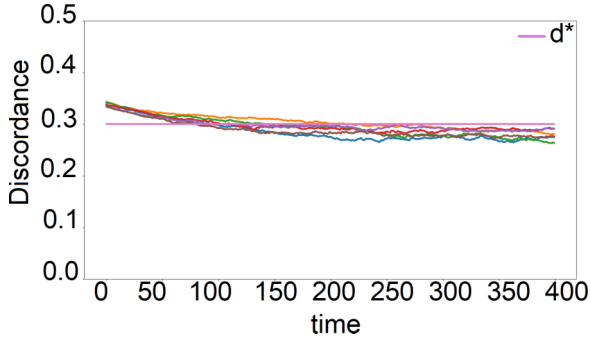

FIG. 7. $(\phi, \beta, \gamma) = (4, 1, 4)$, $K = 800$. Here is a plot of six independent simulations for the discordance d_1. We see that in the metastable regime, discordance maintains and is close to the value computed via block-coordinates (represented as an horizontal pink line on the plot), that is, $d^* = 0.3$.

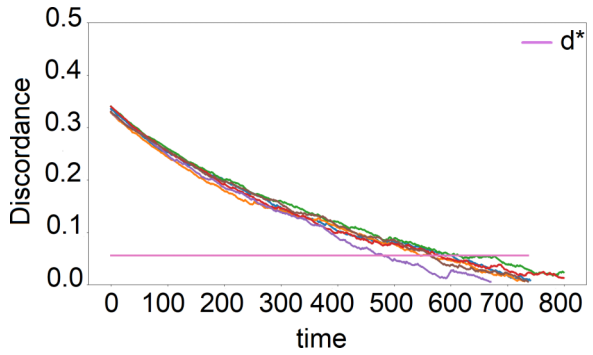

FIG. 8. $(\phi, \beta, \gamma) = (1, 0.8, 1)$, and $K = 800$. Six independent plots have been performed. We see that there is a fast extinction of discordance when $\beta \approx \phi$ (subcritical regime).

$X_k \in \{+1, -1\}^K$ and $A_{lm}, \mathcal{C}^\sigma_{lm}, \mathcal{D}^\sigma_{lm} \in \{0, 1\}$, it is necessary to clarify that $\mathcal{C}^\sigma$ is *roughly equal to* some $c\mathbb{K}$ for $c \in [0, 1]$. Actually, this approximation has to be taken in the *macroscopic viewpoint*, that is, when taking an arbitrary but infinite subset of agents $\{j \in [K] : \frac{j}{K} \in U\}$ for some interval $U \subset [0, 1]$. Sampling this way and taking the associated averages $\overline{X}_U, \overline{A}_{UV}$ defined below, we then obtain, when K tends to $+\infty$, deterministic limits with identical trajectories, regardless of the choice of $U, V \subset [0, 1]$. It is what we call *homogeneity*.

Conjecture 10. Recall that $|U|$ stands for the Lebesgue measure of an interval U in $\mathbb{R}$. Define the partial average,

$$\overline{X}^K_U := \frac{1}{K|U|} \sum_j X_j \mathbb{1}_U\left(\frac{j}{K}\right), \tag{48}$$

for any interval $U \subset [0, 1]$ with $U = [a, b]$, $a < b$. Then, $\overline{X}^K_U$ converges towards a deterministic and continuous trajectory as $K \longrightarrow +\infty$, under the hypothesis that the initial samples $(X_k(0))_{k\in[K]}$ and $(A_{lm})_{l,m}$ are i.i.d. This statement is also valid for the functionals

$$\overline{A}^K_{UV} := \frac{1}{K^2|U||V|} \sum_{lm} A_{lm} \mathbb{1}_{U\times V}\left(\frac{l}{K}, \frac{m}{K}\right). \tag{49}$$

Especially, the global density of links defined as

$$\overline{A}^K = \frac{1}{K^2} \sum_{lm} a_{lm} \tag{50}$$

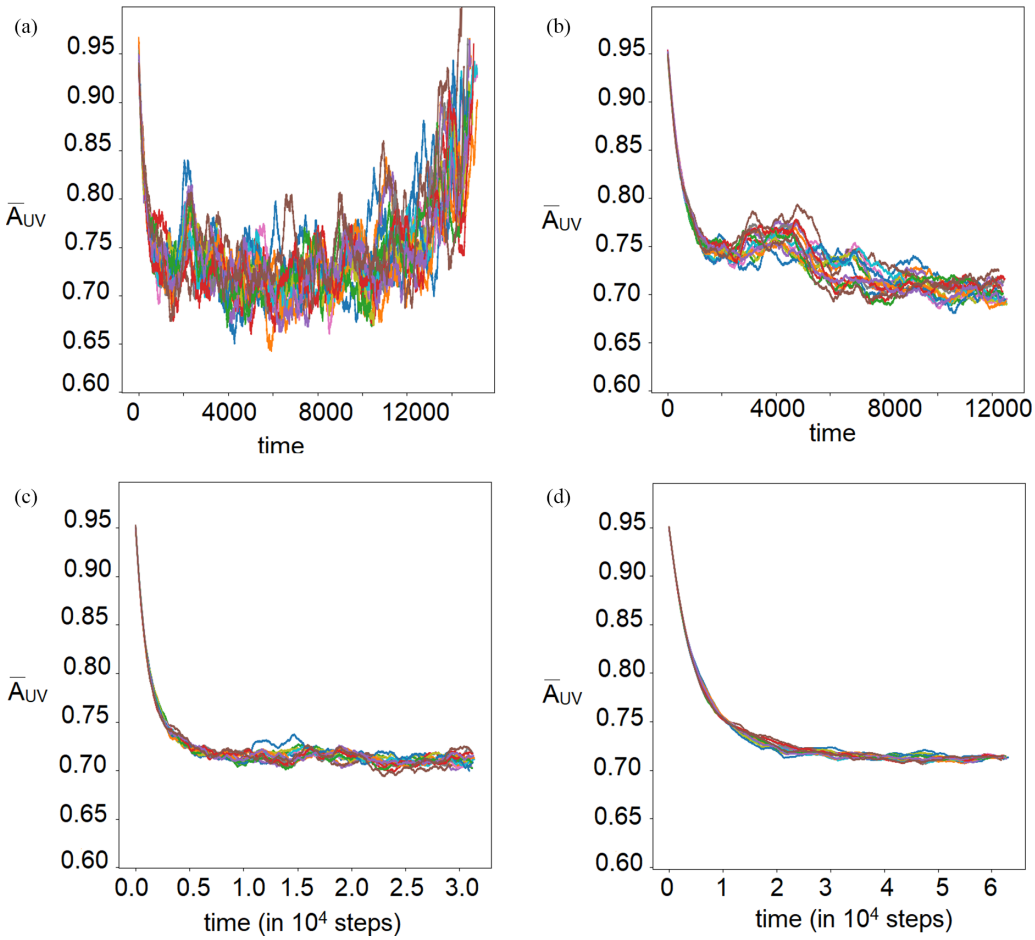

FIG. 9. For several values of K: $K = 120$ in (a), $K = 400$ in (b), $K = 800$ in (c), and $K = 1600$ in (d), we plot the curves of the 16 partial edges means $\{t \mapsto \overline{A}_{UV}(t) : U, V \in \mathcal{P}_4\}$. In all cases, models' parameters are taken constant: $(\phi, \beta, \gamma) = (4, 1, 4)$. At initial times, all random variables are taken i.i.d: $a_{lm}(0) = 1$ with probability 0,95. The concentration of the all trajectories around the same curve when K grows is visible when comparing $K = 120$ (a) and $K = 1600$ (d).

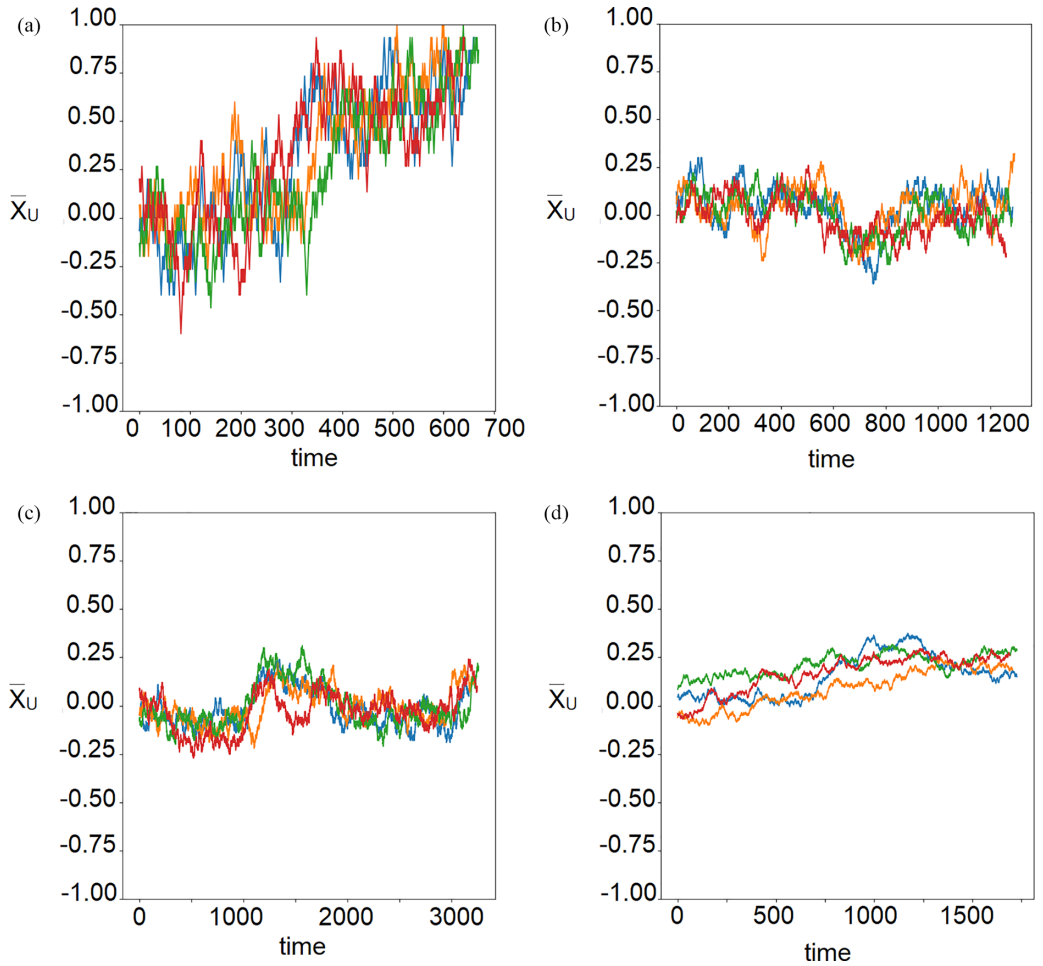

FIG. 10. For several values of K: $K = 120$ in (a), $K = 400$ in (b), $K = 800$ in (c), and $K = 1600$ in (d), we plot the curves of the four partial edges means $\{t \mapsto \overline{X}_U(t) : U \in \mathcal{P}_4\}$, with $(\phi, \beta, \gamma) = (4, 1, 4)$. For all simulations, $x_k(0)$ are taken i.i.d with $x_k(0) = +1$ with probability $\frac{1}{2}$. Here too, a concentration effect occurs, but it is less pronounced because the spin profile includes less variables as the graph.

converges toward a deterministic and continuous trajectory. Furthermore, the limiting trajectories are identical: For any $U, V, U', V' \subset [0, 1]$,

$$\left|\left|\overline{X}^K_U - \overline{X}^K_{U'}\right|\right|_{\infty,T} \longrightarrow 0 \text{ and} \tag{51}$$

$$\left|\left|\overline{A}^K_{UV} - \overline{A}^K_{U'V'}\right|\right|_{\infty,T} \longrightarrow 0, \tag{52}$$

as $K \longrightarrow +\infty$, provided that the entrance sample is i.i.d: $a_{lm}(0) = 1$ with probability a_0 for all l, m, $X_k = +1$ with probability x_0 all variables being independent, and where $||.||_{\infty,T}$ is the uniform norm over the set of bounded real-valued functions defined on the time interval $[0, T]$: $||u|| := \sup_{s\in[0,T]} |u(s)|$.

Remark 11. The hypothesis on the entrance law is crucial. Indeed, suppose that we set $X_k(0) = +1$ with probability 1 for $k < \frac{K}{2}$ and $X_k(0) = -1$ with probability 1 for $k \geqslant \frac{K}{2}$, which is not an i.i.d entrance law. Setting $\beta \gg \phi$ would yield $\overline{X}_{[0,\frac{1}{2}]} \approx +1$ and $\overline{X}_{[\frac{1}{2},1]} \approx -1$, which would contradict the last result.

Remark 12. The type of convergence stated above via partial sampling along intervals $U \in [0, 1]$ has strong links with the cut metric over dense graphs. Roughly speaking, it says that the sequence of random trajectories $(A^K(t))_t$ admits a correctly defined limit object W_t [32].

To verify numerically that the graph displays an homogeneous behavior, we have partitioned the population in four equal parts $I_j := \{k \in [K] : k \equiv j \bmod 4\}$. We thus obtain a partition $\mathcal{P}_4$ of size 4. Then, for $U, V \in \mathcal{P}_4 := (I_j)_{1\leqslant j\leqslant 4}$, we compute the average blockwise defined as

$$\overline{A}_{UV} = \left(\frac{K}{4}\right)^{-2} \sum_{lm} A_{lm} \mathbb{1}_{U\times V}(l, m). \tag{53}$$

We then obtain 16 trajectories. We have performed the simulations for several values of K (see Fig. 9). For increasing K, it is clear that the 16 curves concentrate over the same trajectory and randomness decays. We also display the partial means for the spins: $\overline{X}_U, U \in (I_j)_j$ (see Fig. 10). We observe that the edges means $\overline{A}_{lm}$ converge much faster compared to the spins' ones $\overline{X}_U$ because each average $\overline{A}_{UV}$ contains $(\frac{K}{4})^2 = \frac{K^2}{16}$ terms whereas the spin averages *only* contains $\frac{K}{4}$ terms.

VI. CONCLUSION AND FUTURE WORK

In this paper, we have presented a continuous-time AVM where node and edge steps are not simultaneous. By taking

into account additional permissible configurations, the model is more flexible and satisfactory. Its analysis by the standard NIMFA was refined by a precise change of coordinates using a blockwise approach. Moreover, in the case of dense graphs, a phenomenon that we call *homogeneity* has been conjectured when K becomes large. Although we could not give rigorous proof, numerous numerical simulations were provided to corroborate our intuition. This may be an interesting topic for further investigation. Finally, an alternative interesting research line is to study how connectivity evolves across time, for instance, inspecting the number of connected components. It is a challenging perspective but may significantly contribute to the understanding of dynamical network models.

ACKNOWLEDGMENTS

This work was supported by the Agence Nationale de la Recherche (ANR) through the project NICETWEET (Project No. ANR-20-CE48-0009).

[1] T. M. Liggett, *Interacting Particle Systems* (Springer, 1985), Vol. 2.
[2] C. Castellano, M. A. Muñoz, and R. Pastor-Satorras, Nonlinear q-voter model, Phys. Rev. E **80**, 041129 (2009).
[3] E. Yildiz, A. Ozdaglar, D. Acemoglu, A. Saberi, and A. Scaglione, Binary opinion dynamics with stubborn agents, ACM Trans. Econ. Comput. **1**, 1 (2013).
[4] N. Masuda, Voter models with contrarian agents, Phys. Rev. E **88**, 052803 (2013).
[5] A. Carro, R. Toral, and M. San Miguel, The noisy voter model on complex networks, Sci. Rep. **6**, 24775 (2016).
[6] Y. Dong, M. Zhan, G. Kou, Z. Ding, and H. Liang, A survey on the fusion process in opinion dynamics, Inf. Fusion **43**, 57 (2018).
[7] M. McPherson, L. Smith-Lovin, and J. M. Cook, Birds of a feather: Homophily in social networks, Annu. Rev. Sociol. **27**, 415 (2001).
[8] D. Zillmann and J. Bryant, *Selective Exposure to Communication* (Routledge, New York, 2013).
[9] T. Gross and B. Blasius, Adaptive coevolutionary networks: A review, J. R. Soc. Interface. **5**, 259 (2008).
[10] S. Trajanovski, D. Guo, and P. Van Mieghem, From epidemics to information propagation: Striking differences in structurally similar adaptive network models, Phys. Rev. E **92**, 030801(R) (2015).
[11] T. Raducha, B. Min, and M. San Miguel, Coevolving nonlinear voter model with triadic closure, Europhys. Lett. **124**, 30001 (2018).
[12] N. Malik, F. Shi, H.-W. Lee, and P. J. Mucha, Transitivity reinforcement in the coevolving voter model, Chaos **26**, 123112 (2016).
[13] T. Rogers and T. Gross, Consensus time and conformity in the adaptive voter model, Phys. Rev. E **88**, 030102(R) (2013).
[14] P. Holme and M. E. J. Newman, Nonequilibrium phase transition in the coevolution of networks and opinions, Phys. Rev. E **74**, 056108 (2006).
[15] G. Zschaler, G. A. Böhme, M. Seißinger, C. Huepe, and T. Gross, Early fragmentation in the adaptive voter model on directed networks, Phys. Rev. E **85**, 046107 (2012).
[16] B. Wu, J. Du, and L. Wang, Bridging the gap between opinion dynamics and evolutionary game theory: Some equivalence results, in *2020 39th Chinese Control Conference (CCC)* (IEEE, Chicago, 2020), pp. 6707–6714.
[17] B. Wu, D. Zhou, F. Fu, Q. Luo, L. Wang, and A. Traulsen, Evolution of cooperation on stochastic dynamical networks, PLoS ONE **5**, e11187 (2010).
[18] R. Basu and A. Sly, Evolving voter model on dense random graphs, Ann. Appl. Probab. **27**, 1235 (2017).
[19] T. M. Liggett, *Stochastic Interacting Systems: Contact, Voter and Exclusion Processes* (Springer, Berlin, 1999), Vol. 324 .
[20] V. Sood and S. Redner, Voter model on heterogeneous graphs, Phys. Rev. Lett. **94**, 178701 (2005).
[21] M. E. Yildiz, R. Pagliari, A. Ozdaglar, and A. Scaglione, Voting models in random networks, in *2010 Information Theory and Applications Workshop (ITA), Dublin* (IEEE, 2010), pp. 1–7.
[22] N. J. Stroud, Polarization and partisan selective exposure, J. Commun. **60**, 556 (2010).
[23] F. J. Zuiderveen Borgesius, D. Trilling, J. Möller, B. Bodó, C. H. de Vreese, and N. Helberger, Should we worry about filter bubbles? Internet Policy Rev. **5**, 1 (2016).
[24] D. Spohr, Fake news and ideological polarization: Filter bubbles and selective exposure on social media, Bus. Inform. Rev. **34**, 150 (2017).
[25] D. DiFranzo and K. Gloria-Garcia, Filter bubbles and fake news, XRDS: Crossroads **23**, 32 (2017).
[26] E. Jacob, A. Linker, and P. Mörters, Metastability of the contact process on fast evolving scale-free networks, Ann. Appl. Probab. **29**, 2654 (2019).
[27] R. Van Der Hofstad, *Random Graphs and Complex Networks*, La Jolla, CA (IEEE, 2016), Vol. 43.
[28] L. Lovász, *Large Networks and Graph limits* (American Mathematical Society, USA, 2012), Vol. 60.
[29] P. Van Mieghem, The n-intertwined sis epidemic network model, Computing **93**, 147 (2011).
[30] H. Khalil, *Nonlinear Systems* (Prentice-Hall, Upper Saddle River, NJ, 1996), Vol. 3.
[31] W. M. Haddad and V. Chellaboina, Nonlinear dynamical systems and control, in *Nonlinear Dynamical Systems and Control* (Princeton University Press, Princeton, 2011).
[32] C. Borgs, J. T. Chayes, L. Lovász, V. T. Sós, and K. Vesztergombi, Convergent sequences of dense graphs i: Subgraph frequencies, metric properties and testing, Adv. Math. **219**, 1801 (2008).